WAVES IN RECTANGULAR INLET WITH REFLECTING OR ABSORBING WALLS

By Robert A. Dalrymple,[1] Fellow, ASCE, P. A. Martin,[2] and Li Li[3]

ABSTRACT: The behavior of water waves in the vicinity and within an inlet through an idealized barrier island is studied. Two mathematical approaches are used: the first treats the waves in the ocean and bay with Fourier transforms; and the second uses ''buffer'' domains, which permit the far-field waves to be treated by eigenfunction expansions. The first method is used to treat an inlet with reflective vertical sidewalls. In nature, inlets lined with armor stone absorb wave motion; therefore, the second method is used with impedance boundary conditions at the inlet sidewalls to reduce the wave energy propagating down the channel and into the bay. Wave patterns in the inlet can vary significantly with the angle of incident wave and so can the direction of the radiated wave field in the bay.

INTRODUCTION

Inlets situated on coastlines are subject to waves, which affect their navigability and the tranquility of any attached harbors or bays. An inlet system consists of the ocean, a channel through the coastline, and a bay, as shown schematically in Fig. 1. Slots in man-made breakwaters or between large rectangular caissons can also be treated as inlets, but often with much different geometry relative to a wavelength. The mathematical modeling used here is applicable to both, however.

Dalrymple and Martin (1996) examined the interaction of obliquely incident water waves with an infinitely long rectangular inlet on a reflecting shoreline. They assumed that waves in the inlet would be progressive, neglecting any wave motion reflected back from the end of the inlet (at infinity). This is a reasonable assumption for natural inlets, due to the absorption of wave energy into the inlet side walls (Melo and Guza 1991a,b; Dalrymple 1992). The waves in the ocean were treated with a Fourier transform method, and the waves in the inlet were found by an eigenfunction expansion. Their study provided information about the amplitudes of the progressive wave modes within the inlet and showed the complex wave patterns at the mouth of the inlet, including reflection and diffraction.

Here, the inlet is considered to be of finite length, thus permitting an interaction between the waves within the channel and an infinitely large bay, which can lead to reflections back into the channel. Two separate mathematical approaches are taken to solve the problem: the first follows Dalrymple and Martin (1996) with Fourier transforms in the bay and ocean to describe the waves; and the second follows Momoi (1965a,b 1966, 1968), who developed the ''buffer'' method that introduces radial domains at each end of the rectangular inlet. The buffer domains permit expressing the ocean and bay wave fields by polar eigenfunction expansions, thus removing the need to compute difficult Fourier transforms (particularly for the case of absorbing channel sidewalls). The cost is the added complexity of determining the eigenfunction expansions in the two additional buffer domains.

First, the Fourier transform method is used to examine purely reflective channel sidewalls. Oblique wave incidence is handled by separating the problem into symmetric and antisymmetric problems. In the second half of the paper, the buffer domain method is used (for normally incident waves), and an impedance boundary condition at the sidewalls of the channel is demonstrated.

For both problems, a semi-infinite ocean, $x < 0$, connected to a semi-infinite bay, $x > \ell$, by a rectangular channel of length ℓ and width $2b$, $-b < y < b$, is considered. The shortlines, at $x = 0$ and $x = \ell$ for $|y| > b$, and the channel walls, $|y| = b$ for $0 < x < \ell$, are assumed to be vertical and perfectly reflecting. A schematic is shown in Fig. 1. A plane wave in the ocean is obliquely incident on the shore; the problem is to determine the reflected waves and the waves that pass through the channel and radiate out into the bay.

For water of constant depth, the above problem reduces to a series of boundary-value problems for the Helmholtz equation, one for each region: ocean, inlet, and bay. For the second method (Momoi's), two additional domains are introduced at each end of the channel, to allow the use of polar coordinates offshore and in the bay. The first approach here uses Fourier transforms to express the ocean waves and bay waves, in the second approach, Hankel expansions are used.

REFLECTING SIDEWALLS AND FOURIER TRANSFORM METHOD

Theoretical Considerations

The problem has been described above (see the schematic layout in Fig. 1). One solves it by separating the water into three regions, namely, the ocean, channel, and bay. It was solved here using Fourier integrals in the ocean and in the bay, combined with a modal expansion in the channel; the unknown coefficients are determined by imposing matching conditions at the two ends of the channel and solving a matrix equation. This method has been used previously by Mendez et al. (1983) in the context of 2D electromagnetics (scattering of a TE-wave by a slit in a thick perfectly conducting screen). Park et al. (1994) extended the method, so that the wave number in the channel differs from that in the ocean and bay (corresponding to water of different constant depths). The work in the present study differs in three respects. First, efficient formulas are used for the computation of the matrix entries (they are all reduced to finite integrals). Second, effective asymptotic approximations are obtained for long waves (short waves are more appropriate for electromagnetic applications). Third, the present study concentrates on calculating the wave pattern in the vicinity of the channel rather than the waves in the far field.

In the ocean, $x < 0$, the velocity potential governing the wave motion can be written as follows:

[1]Davis Prof. of Civ. and Envir. Engrg., Ctr. for Appl. Coast. Res., Univ. of Delaware, Newark, DE 19716.

[2]Prof. of Math. and Comp. Sci., Colorado School of Mines, Golden, CO 80401.

[3]Grad. Student, Ctr. for Appl. Coast. Res., Univ. of Delaware, Newark, DE.

Note. Discussion open until May 1, 2001. To extend the closing date one month, a written request must be filed with the ASCE Manager of Journals. The manuscript for this paper was submitted for review and possible publication on May 13, 1998. This paper is part of the ***Journal of Waterway, Port, Coastal, and Ocean Engineering***, Vol. 126, No. 6, November/December, 2000. ©ASCE, ISSN 0733-950X/00/0006-0288–0296/$8.00 + $.50 per page. Paper No. 18379.

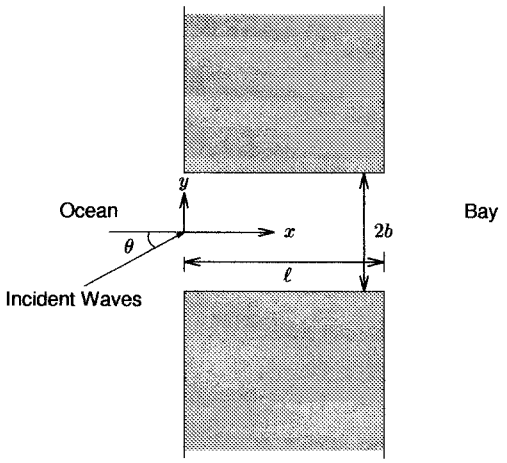

FIG. 1. Schematic Diagram of Inlet in Infinitely Large Barrier

$$\Phi_1(x, y, z, t) = \text{Re}\left\{\phi_1(x, y)\frac{\cosh k(h + z)}{\cosh kh}e^{-i\omega t}\right\}$$

where the wave number k and the angular frequency ω are related to the water depth h by the usual (frequency) dispersion relationship, which involves the gravitational acceleration g.

$$\omega^2 = gk \tanh kh$$

Here, z is the vertical coordinate, with the mean free surface at $z = 0$ and the rigid bottom at $z = -h$. Here, ϕ_1 is decomposed as

$$\phi_1 = \phi_{\text{inc}} + \phi_{\text{ref}} + \phi_1^s + \phi_1^a$$

where

$$\phi_{\text{inc}} = pe^{ik(y\sin\theta + x\cos\theta)}$$

gives the incident wave potential propagating at an angle θ to the x-axis, where p is a dimensional constant. The corresponding wave height H is $2i\omega p/g$, and the free surface elevation is

$$\eta = -\frac{i\omega}{g}\text{Re}(\phi_1 e^{-i\omega t})$$

The reflected wave is

$$\phi_{\text{ref}} = pe^{ik(y\sin\theta - x\cos\theta)}$$

and $\phi_1^s + \phi_1^a$ gives the wave radiating out to the ocean from the channel due to the interaction of the incident waves and the channel. Rearranging $\phi_{\text{inc}} + \phi_{\text{ref}}$ yields

$$\phi_{\text{inc}} + \phi_{\text{ref}} = 2p\cos(ky\sin\theta)\cos(kx\cos\theta) + 2ip\sin(ky\sin\theta)\cos(kx\cos\theta) \quad (1)$$

which is the sum of two standing-wave patterns, one symmetric and the other antisymmetric about the x-axis. The solution procedure is therefore split into two parts, one associated with the symmetric problem (superscript s) and one associated with the antisymmetric problem (superscript a). The following Fourier integrals are associated with these two problems, respectively (Sneddon 1995):

$$\phi_1^s = \frac{1}{\pi}\int_0^\infty A^s(\lambda)e^{-i\beta(\lambda)x}\cos\lambda y\, d\lambda \quad (2)$$

$$\phi_1^a = \frac{1}{\pi}\int_0^\infty A^a(\lambda)e^{-i\beta(\lambda)x}\sin\lambda y\, d\lambda \quad (3)$$

for $x < 0$, where

$$\beta(\lambda) = \begin{cases}\sqrt{k^2 - \lambda^2}, & 0 \le \lambda \le k\\ i\sqrt{\lambda^2 - k^2}, & \lambda > k\end{cases} \quad (4)$$

The magnitudes of $A^s(\lambda)$ and $A^a(\lambda)$ are to be determined by matching to the wave solution in the channel.

Within the channel of width $2b$ and length ℓ, the wave potential is

$$\Phi_2(x, y, z, t) = \text{Re}\left\{\phi_2(x, y)\frac{\cosh k(h + z)}{\cosh kh}e^{-i\omega t}\right\}$$

where $\phi_2 = \phi_2^s + \phi_2^a$

$$\phi_2^s = \sum_{n=0}^{\infty}(\xi_{2,n}^s e^{i\beta(\lambda_n^s)x} + \bar{\xi}_{2,n}^s e^{-i\beta(\lambda_n^s)(x-\ell)})\cos\lambda_n^s y \quad (5)$$

$$\phi_2^a = \sum_{n=0}^{\infty}(\xi_{2,n}^a e^{i\beta(\lambda_n^a)x} + \bar{\xi}_{2,n}^a e^{-i\beta(\lambda_n^a)(x-\ell)})\sin\lambda_n^a y \quad (6)$$

for $0 \le x \le \ell$, $-b < y < b$

$$\lambda_n^s = n\pi/b; \quad \lambda_n^a = \left(n + \frac{1}{2}\right)\pi/b$$

The boundary condition at the vertical sidewalls is specified as

$$\frac{\partial\phi}{\partial y} = i\gamma\phi \quad \text{at } |y| = b \quad (7)$$

When $\gamma = 0$, this is a no-flow boundary condition. When $\gamma \neq 0$, it is an impedance boundary condition, which is used later in the third section to absorb wave energy (Dalrymple 1992).

The first terms in the summation for ϕ_2^s represent waves propagating down the straight channel; the second terms are waves that are reflected back from the bay end of the channel. For $n = 0$, the waves propagate directly down the centerline, and the remaining waves propagate down the channel obliquely, reflecting from the vertical sidewalls. For values of n, such that $\lambda_n^s > k$, these waves decay in the propagation direction. A similar interpretation of ϕ_2^a can be made.

In the bay, $x > \ell$, the wave field is again represented by a Fourier integral

$$\Phi_3(x, y, z, t) = \text{Re}\left\{\phi_3(x, y)\frac{\cosh k(h + z)}{\cosh kh}e^{-i\omega t}\right\}$$

where, again, the total solution is decomposed into symmetric and antisymmetric parts, $\phi_3 = \phi_3^s + \phi_3^a$

$$\phi_3^s = \frac{1}{\pi}\int_0^\infty B^s(\lambda)e^{i\beta(\lambda)(x-\ell)}\cos\lambda y\, d\lambda \quad (8)$$

$$\phi_3^a = \frac{1}{\pi}\int_0^\infty B^a(\lambda)e^{i\beta(\lambda)(x-\ell)}\sin\lambda y\, d\lambda \quad (9)$$

To determine the forms of $A^\alpha(\lambda)$, $B^\alpha(\lambda)$, $\xi_{2,n}^\alpha$, and $\bar{\xi}_{2,n}^\alpha$ for $\alpha = s, a$, four matching conditions are used. The first two are satisfied at the mouth of the channel ($x = 0$); the second pair is applied at the entrance to the bay ($x = \ell$).

The first matching condition requires that the vehicles in the x-direction be the same in the ocean and the channel

$$\frac{\partial\phi_2}{\partial x} = \frac{\partial\phi_1}{\partial x} \quad \text{at } x = 0, \quad |y| < b \quad (10)$$

The second requirement is that the pressure be continuous across the channel mouth, which can be expressed as

$$\phi_2 = \phi_1 \quad \text{at } x = 0, \quad |y| < b$$

At the other end of the channel, there are similar relations between ϕ_2 and ϕ_3

$$\frac{\partial \phi_2}{\partial x} = \frac{\partial \phi_3}{\partial x} \quad \text{at } x = \ell,\ |y| < b \tag{11}$$

$$\phi_2 = \phi_3 \quad \text{at } x = \ell,\ |y| < b \tag{12}$$

Finally, there are the reflecting shoreline conditions

$$\frac{\partial \phi_1}{\partial x} = 0 \quad \text{at } x = 0, \quad |y| > b$$

$$\frac{\partial \phi_3}{\partial x} = 0 \quad \text{at } x = \ell, \quad |y| > b$$

From now on, it is sufficient to examine only $y \geq 0$.

Symmetric Problem

This portion of the problem involves all of the symmetric parts of ϕ_1^s, ϕ_2^s, and ϕ_3^s. The first matching condition [(10)] leads to

$$-\frac{i}{\pi}\int_0^\infty A^s(\lambda)\beta(\lambda)\cos \lambda y\, d\lambda = \begin{cases} \displaystyle\sum_{n=0}^{\infty} i\beta(\lambda_n^s)(\xi_{2,n}^s - \bar{\xi}_{2,n}^s\gamma_n^s)\cos \lambda_n^s y, \\ \quad \text{for } 0 \leq y \leq b \\ 0, \quad \text{for } y > b \end{cases} \tag{13}$$

where

$$\gamma_n^s = \exp(i\beta(\lambda_n^s)\ell)$$

which is not to be confused with γ in the impedance boundary condition.

Inverting the Fourier cosine transform, one obtains

$$A^s(\lambda) = -\sum_{n=0}^{\infty}(\xi_{2,n}^s - \bar{\xi}_{2,n}^s\gamma_n^s)\frac{\beta(\lambda_n^s)}{\beta(\lambda)}\mathcal{L}_n^s(\lambda) \tag{14}$$

where

$$\mathcal{L}_n^s(\lambda) = 2\int_0^b \cos \lambda_n^s y \cos \lambda y\, dy = \frac{2(-1)^n \lambda \sin \lambda b}{\lambda^2 - (\lambda_n^s)^2} \tag{15}$$

and $\mathcal{L}_n^s(\lambda)$ is well defined for all λ, including $\lambda = \lambda_n^s$.

The second matching condition, including the definition of $A^s(\lambda)$, leads to

$$\sum_{n=0}^{\infty}(\xi_{2,n}^s + \bar{\xi}_{2,n}^s\gamma_n^s)\cos \lambda_n^s y = 2p\cos(ky \sin \theta) - \frac{1}{\pi}\int_0^\infty \sum_{n=0}^{\infty}(\xi_{2,n}^s - \bar{\xi}_{2,n}^s\gamma_n^s)\beta(\lambda_n^s)\frac{\mathcal{L}_n^s(\lambda)}{\beta(\lambda)}\cos \lambda y\, d\lambda$$

for $0 \leq y < b$. Using the orthogonality of $\{\cos \beta(\lambda_n^s)y\}$ over the range $0 \leq y \leq b$ removes the y dependency in this equation and provides an equation for a_m^s and b_m^s

$$b(a_m^s + b_m^s\gamma_m^s) = \varepsilon_m p\mathcal{L}_m^s(k \sin \theta) - \frac{1}{2}\varepsilon_m \sum_0^\infty (\xi_{2,n}^s - \bar{\xi}_{2,n}^s\gamma_n^s)\beta(\lambda_n^s)D_{mn}^s, \quad m = 1, 2, 3, \ldots \tag{16}$$

where $\varepsilon_0 = 1$, $\varepsilon_m = 2$ for $m > 0$, and

$$D_{mn}^s = D_{nm}^s = \frac{1}{\pi}\int_0^\infty \mathcal{L}_m^s(\lambda)\mathcal{L}_n^s(\lambda)\frac{d\lambda}{\beta(\lambda)} \tag{17}$$

Now, there are two similar matching conditions at $x = \ell$. Requiring that the velocities in the bay match those in the channel or the shoreline, one obtains

$$\frac{i}{\pi}\int_0^\infty B^s(\lambda)\beta(\lambda)\cos \lambda y\, d\lambda = \begin{cases} \displaystyle\sum_{n=0}^{\infty} i\beta(\lambda_n^s)(\xi_{2,n}^s\gamma_n^s - \bar{\xi}_{2,n}^s)\cos \lambda_n^s y, \\ \quad \text{for } 0 \leq y \leq b \\ 0, \quad \text{for } y > b \end{cases}$$

A Fourier cousine transform in y yields

$$B^s(\lambda) = \sum_{n=0}^{\infty}(\xi_{2,n}^s\,\gamma_n^s - \bar{\xi}_{2,n}^s)\frac{\beta(\lambda_n^s)}{\beta(\lambda)}\mathcal{L}_n^s(\lambda) \tag{18}$$

Substituting $B^s(\lambda)$ into (8) gives

$$\phi_3^s(x, y) = \frac{1}{\pi}\int_0^\infty \sum_{n=0}^{\infty}(\xi_{2,n}^s\gamma_n^s - \bar{\xi}_{2,n}^s)\frac{\beta(\lambda_n^s)}{\beta(\lambda)}\mathcal{L}_n^s(\lambda)e^{i\beta(\lambda)(x-\ell)}\cos \lambda y\, d\lambda \tag{19}$$

The last matching condition is (12). Applying it, using the orthogonality of $\{\cos \lambda_n^s y\}$ again, gives

$$b(a_m^s\gamma_m^s + b_m^s) = \frac{1}{2}\varepsilon_m \sum_{n=0}^{\infty}\beta(\lambda_n^s)(\xi_{2,n}^s\gamma_n^s - \bar{\xi}_{2,n}^s)D_{mn}^s, \quad m = 0, 1, 2, \ldots \tag{20}$$

To obtain solutions, one truncates the series representation of ϕ_2^s at $n = N$ and then takes (16) and (20) from $m = 0$ to N. This gives the following $(2N + 2) \times (2N + 2)$ set of equations for a_m^s and b_m^s, $m = 0, 1, \ldots, N$:

$$\sum_{n=0}^{N}\{\xi_{2,n}^s\Gamma_{mn}^+ + \bar{\xi}_{2,n}^s\gamma_n^s\Gamma_{mn}^-\} = 2p\varepsilon_m\mathcal{L}_m^s(k \sin \theta)$$

$$\text{for } m = 0, 1, 2, \ldots, N \tag{21}$$

$$\sum_{n=0}^{N}\{\xi_{2,n}^s\gamma_n^s\Gamma_{mn}^- + \bar{\xi}_{2,n}^s\Gamma_{mn}^+\} = 0 \quad \text{for } m = 0, 1, 2, \ldots, N \tag{22}$$

where

$$\Gamma_{mn}^{\pm} = 2b\delta_{mn} \pm \varepsilon_m\beta(\lambda_n^s)D_{mn}^s$$

Here $\delta_{mn} = 1$ for $m = n$ and is zero otherwise.

Antisymmetric Problem

The antisymmetric problem is treated in the same manner as the symmetric problem. The terms $A^a(\lambda)$ and $\mathcal{L}_n^a$ are given by

$$A^a(\lambda) = -\sum_{n=0}^{\infty}(\xi_{2,n}^a - \bar{\xi}_{2,n}^a\gamma_n^a)\frac{\beta(\lambda_n^a)}{\beta(\lambda)}\mathcal{L}_n^a(\lambda) \tag{23}$$

$$\mathcal{L}_n^a(\lambda) = 2\int_0^b \sin \lambda_n^a y \sin \lambda y\, dy = \frac{2(-1)^{n+1}\lambda \cos \lambda b}{\lambda^2 - (\lambda_n^a)^2} \tag{24}$$

where

$$\gamma_n^a = \exp\{i\beta(\lambda_n^a)\ell\}$$

From the two matching conditions at the ocean end of the channel, one obtains

$$b(a_m^a + b_m^a\gamma_m^a) = 2pi\mathcal{L}_m^a(k \sin \theta) - \sum_{n=0}^{\infty}(\xi_{2,n}^a - \bar{\xi}_{2,n}^a\gamma_n^a)\beta(\lambda_n^a)D_{mn}^a, \quad m = 1, 2, \ldots \tag{25}$$

where

$$D_{mn}^a = D_{nm}^a = \frac{1}{\pi}\int_0^\infty \mathcal{L}_m^a(\lambda)\mathcal{L}_n^a(\lambda)\frac{d\lambda}{\beta(\lambda)} \tag{26}$$

The coefficients D_{mn}^a and D_{mn}^s are provided in more convenient form in Appendix I.

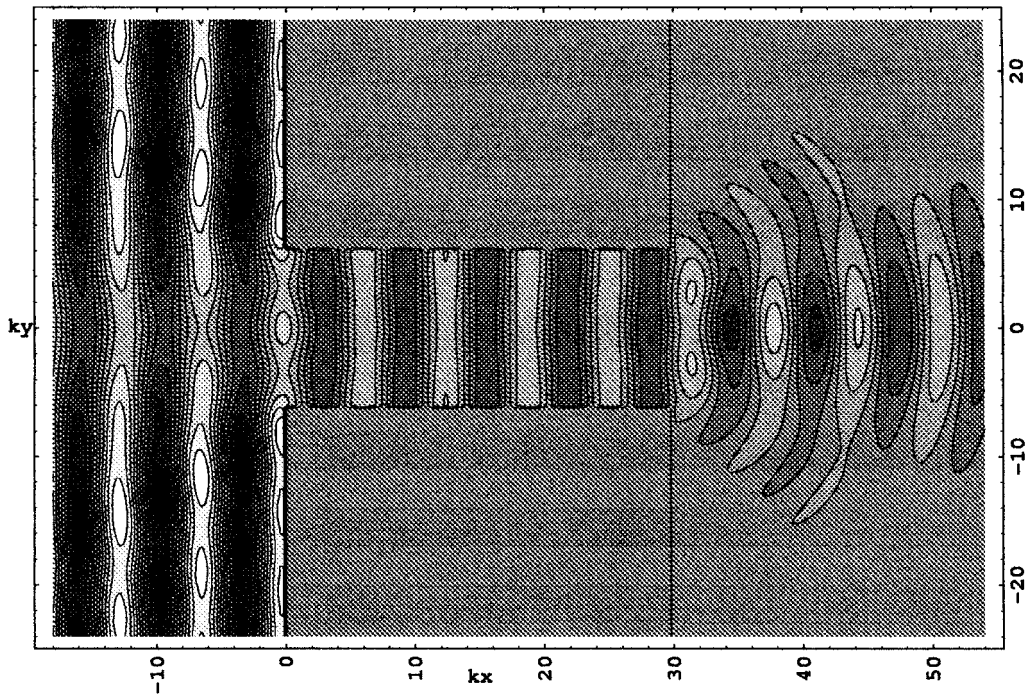

FIG. 2. Wave Train Normally Incident to Inlet; $kb = 6$, $k\ell = 30$

The conditions at the bay end of the channel give

$$b(a_m^a\gamma_m^a + b_m^a) = \sum_{n=0}^{\infty} \beta(\lambda_n^a)(\xi_{2,n}^a\gamma_n^a - \bar{\xi}_{2,n}^a)D_{mn}^a, \quad m = 0, 1, 2, \ldots \tag{27}$$

Again, truncating ϕ_2^a and the above systems [(25) and (27)] gives the following $(2N + 2) \times (2N + 2)$ matrix equation for the antisymmetric solution:

$$\sum_{n=0}^{N} \{\xi_{2,n}^a\Delta_{mn}^+ + \bar{\xi}_{2,n}^a\gamma_n^a\Delta_{mn}^-\} = 2pi\mathcal{L}_m^a(k \sin\theta)$$

$$\text{for } m = 0, 1, 2, \ldots, N \tag{28}$$

$$\sum_{n=0}^{N} \{\xi_{2,n}^a\gamma_n^a\Delta_{mn}^- + \bar{\xi}_{2,n}^a\Delta_{mn}^+\} = 0 \quad \text{for } m = 0, 1, 2, \ldots, N \tag{29}$$

where

$$\Delta_{mn}^{\pm} = b\delta_{mn} \pm \beta(\lambda_n^a)D_{mn}^a$$

Results

The solution procedure involves inverting the complex matrices [(21) and (22)] and [(28) and (29)]. The coefficients D_{nm}^s and D_{nm}^a are determined as shown in Appendix A of Dalrymple and Martin (1996) using a 150-point Gauss quadrature. The matrices are inverted using the subroutine LEQT1C of the IMSL (a FORTRAN mathematical and statistics library). The coefficient $\xi_{2,n}^s$ and $\xi_{2,n}^a$ are very stable for $N \geq 15$, $(\|\xi_{2,0_{N+1}}^s| - |\xi_{2,0_N}^s\|)/|\xi_{2,0_N}^s| < 0.00015$ and $(\|\xi_{2,0_{N+1}}^a| - |\xi_{2,0_N}^a\|)/|\xi_{2,0_N}^a| < 6.10^{-6}$. For all cases, $N = 15$.

Fig. 2 shows the instantaneous water surface for a wave train normally incident on a channel. The dimensionless width of the channel is $kb = 6$, and the length of the channel $k\ell = 30$. In terms of relative dimensions, all distances have been nondimensionalized by k. On the ocean side of the channel (left side of Fig. 2), the reflective ocean shoreline leads to a standing-wave system, except in front of the channel, where the waves are partially standing due to the weak reflection from the channel mouth. Within the channel the waves propagate straight through the channel to the bay. On the bay side, there is a focusing of the waves just after the channel exit, and then diffraction spreads the wave energy within the bay. The focusing of the waves within the bay is due to the diffraction from each corner of the channel.

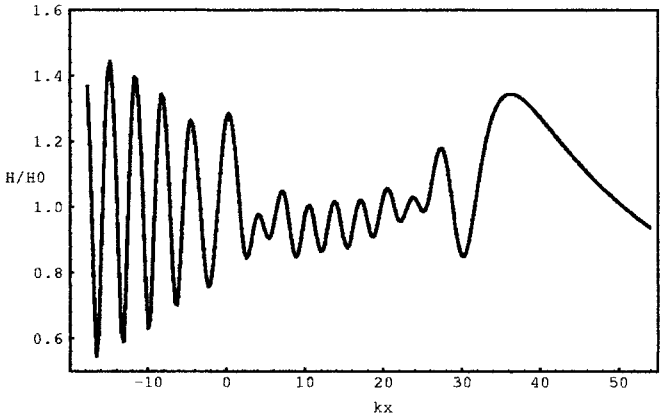

FIG. 3. Nondimensional Wave Envelope for Wave Train Normally Incident to Inlet; $kb = 6$, $k\ell = 30$ [Solid Line = Centerline ($y = 0$)]

The envelope of wave heights $H(x)/H_0$ along the centerline of the channel, $y = 0$, is shown in Fig. 3. The partial standing wave on the ocean side of the channel is clearly shown. Within the channel, the wave envelope is oscillatory due to a partial standing-wave system, due to reflections from the two transitions: inlet-to-bay and inlet-to-ocean.

Fig. 4 shows a wave train incident on the same channel at 22.8° angle of incidence, which satisfies the geometric condition $\theta = \tan^{-1}(2b/\ell)$, leading to the wave train exiting the channel at an angle opposite to the incident angle. Within the ocean, the obliquely reflected waves from the shoreline lead to a short-crested sea state, except in the vicinity of the channel mouth, where the reflection is weak, resulting in longer crested waves. The envelope of wave heights $H(x)/H_0$ along the cen-

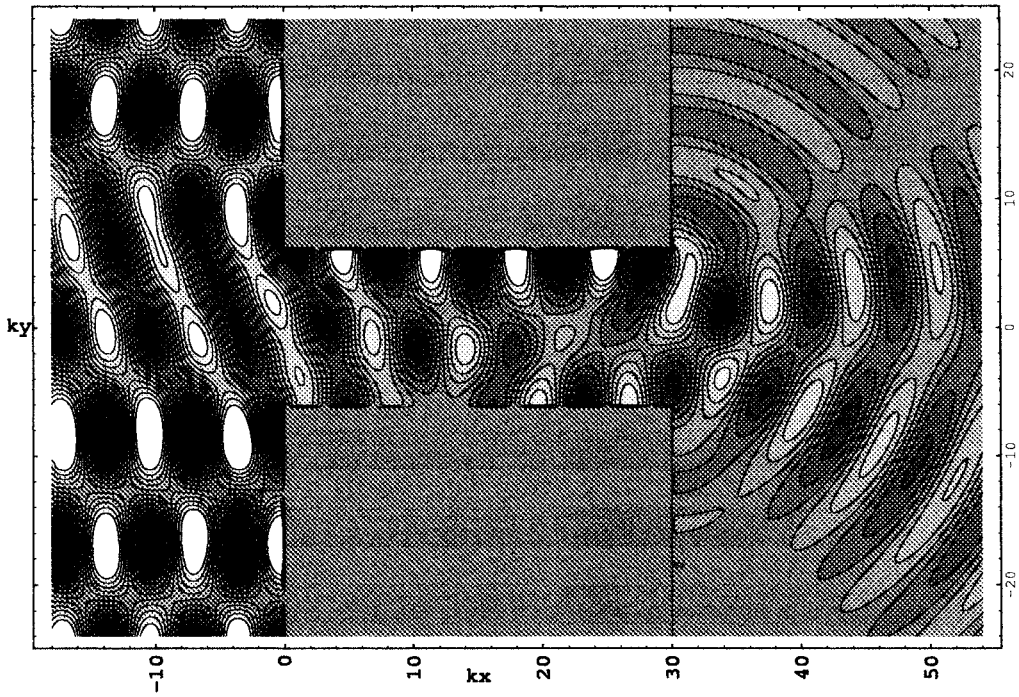

FIG. 4. Wave Train Incident at 22.8° to Inlet; $kb = 6$, $k\ell = 30$ [Note Intensification of Wave at $ky = 6$ due to Sidewall Reflection]

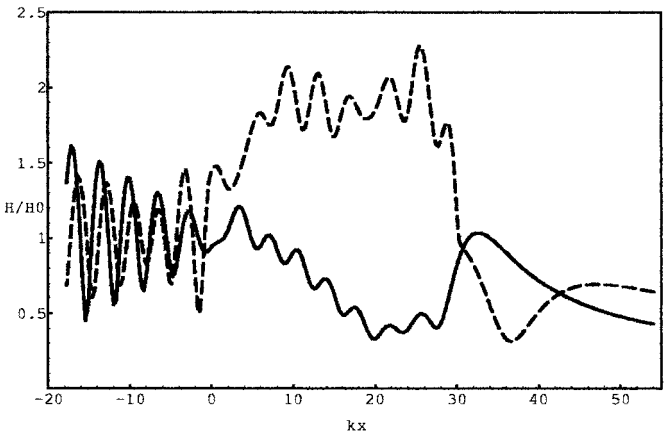

FIG. 5. Nondimensional Wave Envelope for Wave Train Incident at 22.8° to Inlet; $kb = 6$, $k\ell = 30$ [Solid Line Is Wave Amplitude at Centerline ($y = 0$), Dashed Line Is Envelope at $y = b$]

terline of the channel, $y = 0$, is shown in Fig. 5 as the solid line. There is a rapid decrease in wave amplitude within the channel as the waves are directed into the channel wall at $y = +b$, leaving the centerline in the geometric shadow zone as the waves diffract from the channel mouth ($x = 0$, $y = -b$ in Fig. 1). The dashed line in the figure shows the wave amplitude along the wall at $y = +b$. The rapid decay within the bay is also shown for both locations.

Fig. 6 shows the instantaneous water surface for a wave train incident on the same channel at 45°. The reflected waves from the shoreline diffract into the reflection shadow zone from the inlet, so that far upwave of the inlet the waves are once again short-crested. Within the channel, the reflection from the sidewalls and the diffraction from the upwave side of the channel mouth are also clear. Finally, the wave train, after undergoing reflections within the channel, exits the channel in about the same direction as the incident wave train in the ocean, although waves radiate in other directions as well. For a fixed angle of wave incidence, the principal direction of the radiated waves in the bay is directly due to the channel length and the number of reflections that take place within the channel.

Fig. 7 shows the normalized wave amplitude along the x-axis, beginning from offshore, down the centerline of the channel, and into the bay. The standing-wave system in front of the channel is clearly seen on the left in Fig. 7 and the wave heights within the channel are roughly the same amplitude, with an oscillation due to the reflections of the waves from the transitions. There is a rapid decrease in centerline wave height within the bay, as the waves are radiating in a different direction than the x-axis.

The amount of wave energy entering the bay is an important quantity for design. This quantity $\mathcal{T}_E$ is defined here as the wave flux leaving the channel at $x = \ell$ divided by the energy flux contained in a crest length of $2b$ of the incident wave train. The ϕ part of the wave energy flux across a line of width $2b$ is defined as follows (Stoker 1957):

$$\rho \, \mathrm{Im} \left\{ \int_{-b}^{b} \phi^* \frac{\partial \phi}{\partial n} \, dy \right\}$$

where ρ = fluid density; and n = normal direction across the line. Due to the orthogonality of the eigenfunctions across the channel, $\mathcal{T}_E$ can be separated into symmetric and antisymmetric parts,

$$\mathcal{T}_E = \mathcal{T}_E^s + \mathcal{T}_E^a \tag{30}$$

where

$$\mathcal{T}_E^s = |\xi_{2,0}|^2 - |\bar{\varepsilon}_{2,0}|^2 + \frac{1}{2k} \sum_{n=1} (\mathrm{Re}\{\beta(\lambda_n^s)\}(|\xi_{2,n}^s|^2|\gamma_n^s|^2 - |\bar{\xi}_{2,n}^s|^2) + 2 \, \mathrm{Im}\{\beta(\lambda_n^s)\}\mathrm{Im}\{\bar{\xi}_{2,n}^{s*} \xi_{2,n}^s \gamma_n^s\})$$

$$\mathcal{T}_E^a = \frac{1}{2k} \sum_{n=0} (\mathrm{Re}\{\beta(\lambda_n^a)\}(|\xi_{2,n}^a|^2|\gamma_n^s|^2 - |\bar{\xi}_{2,n}^a|^2) + 2 \, \mathrm{Im}\{\beta(\lambda_n^a)\}\mathrm{Im}\{\bar{\xi}_{2,n}^{a*} \xi_{2,n}^a \gamma_n^a\}) \tag{31}$$

The first terms in each of the summations are nonzero for the progressive wave modes. The evanescent modes are ac-

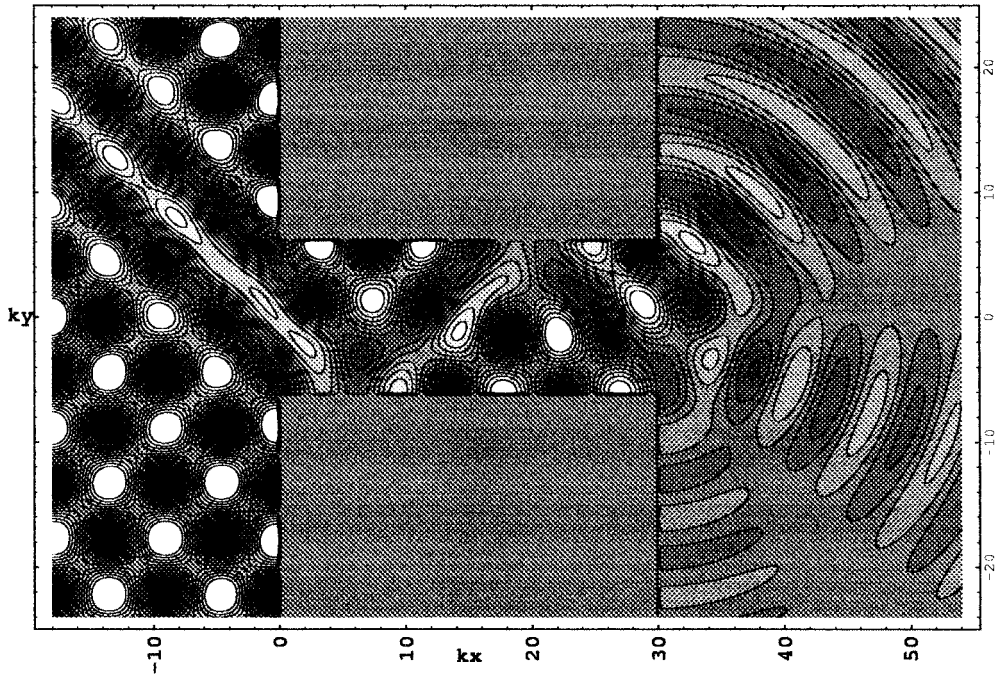

FIG. 6. Wave Train Incident at 45° to Inlet; $kb = 6$, $k\ell = 30$

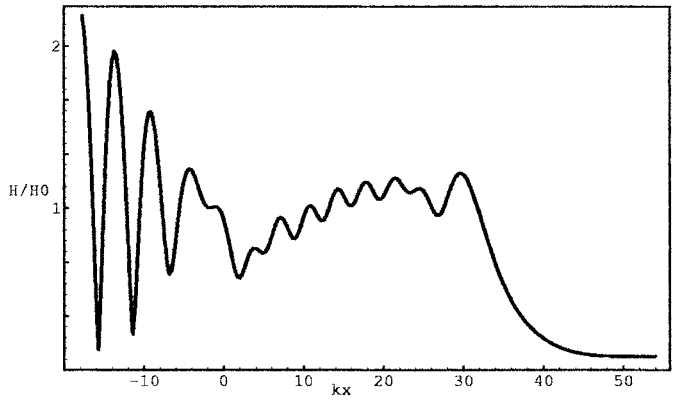

FIG. 7. Centerline Wave Envelope for Wave Train Incident at 45° to Inlet; $kb = 6$, $k\ell = 30$

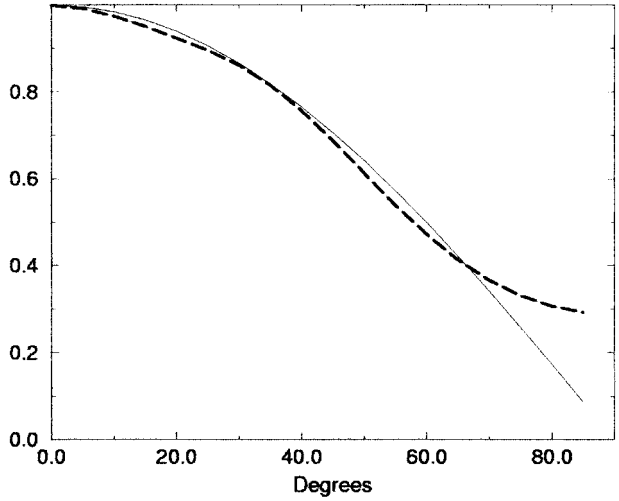

FIG. 8. $\mathcal{T}_E$ (Dashed Line) and Cosine θ (Solid Line) as Function of Angle of Wave Incidence to Shoreline

counted for by the second set of terms in the summations. For long channels, these terms decay and do not contribute.

For the plane wave approximation, given in (49)

$$\mathcal{T}_E = \frac{4P(\mathcal{L}_0^s(k \sin \theta))^2}{b^2((1 + P)^4 - 2(1 - P)^2(1 + P)^2 \cos 2k\ell + (1 - P)^4)} \tag{32}$$

For the two examples, shown in Figs. 4 and 6, $\mathcal{T}_E$ is equal to 0.909 and 0.689, respectively. The major reason for a reduction of $\mathcal{T}_E$ from unity is that the projection of a section of obliquely incident wave crest onto the shoreline illuminates a longer section of coast than the crest length, except at normal incidence. For a crest length of $2b$ approaching at an angle θ, the illuminated shoreline is $2b/\cos\theta$ from a simple geometric argument. An inlet of width $2b$ only intercepts $2b \cos\theta$ of the wave crest. For example, a wave approaching at 90° would not illuminate the inlet at all (except by diffraction). A simple approximation to $\mathcal{T}_E$ is cos θ. For the two examples above, cos θ is 0.922 and 0.707, respectively. Clearly, reflection of wave energy offshore by reflection at the channel and bay mouths, accounts for very little. In Fig. 8, $\mathcal{T}_E$ is compared to cos θ, showing that only at large angles is there a difference due to diffraction of the oblique waves into the inlet.

ABSORBING SIDEWALLS AND MOMOI'S METHOD

Theory

Another way to solve the ocean-channel-bay problem is based on Momoi's buffer domain method (Momoi 1965a,b, 1966, 1968), which does not use Fourier transforms and hence does not result in complicated integrals. For this reason, with energy absorbing sidewalls, it becomes more convenient to use it rather than the eigenfunction expansion approach.

Now, let the whole domain be separated into five parts as shown in Fig. 9; namely, the ocean; the ocean buffer domain, which is a semicircular domain on the horizontal plane; the channel; the bay buffer domain; and the bay of infinite size. In the ocean, ($x < 0$, $r > b$, $0 < \theta_O < \pi$), b is the half-channel width, as before, $\theta_O = \tan^{-1}(|x|/y)$, $r = \sqrt{x^2 + y^2}$, and the velocity potential governing the wave motion in the ocean can be written as before [(1)].

The dimensionless potential ϕ_1 is decomposed as

$$\phi_1 = \phi_{inc} + \phi_{ref} + \phi_{1r} \tag{33}$$

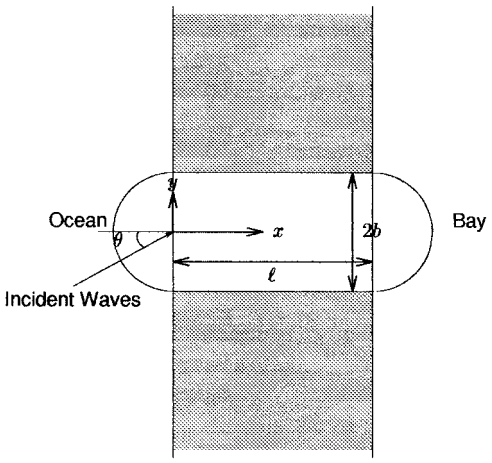

FIG. 9. Schematic Diagram of Inlet, with Two Semicircular Buffer Domains at Channel Entrance and Exit

where as before ϕ_{inc} = incident wave train [(1)]; and ϕ_{ref} = wave train reflected from the shoreline [(1)]. The third term, ϕ_{1r}, gives the wave radiating from the channel, which will be expressed in a Hankel expansion

$$\phi_{1r} = \sum_{n=0}^{\infty} \xi_1^{2n} \cos(2n\theta_o) H_{2n}^1(kr)$$

For normally incident waves, the only ones treated here are

$$\phi_{inc} + \phi_{ref} = 2p \cos(kx)$$

Using the Bessel expansion of the cosine, one has

$$\phi_{inc} + \phi_{ref} = 2p \sum_{n=0}^{\infty} \varepsilon_n \cos(2n\theta_O) J_{2n}(kr)$$

where $\varepsilon_0 = 1$ and $\varepsilon_n = 2$ ($n \geq 1$).

The forms of ξ_1^{2n} are to be determined by matching to the wave solution in the buffer domain.

In the buffer domain of the ocean ($x < 0$, $0 < r < b$, $0 < \theta_O < \pi$), the velocity potential governing the wave motion can be written as follows:

$$\Phi_4(x, y, z, t) = \text{Re}\left\{\phi_4(x, y) \frac{\cosh k(h + z)}{\cosh(kh)} e^{-i\omega t}\right\}$$

where

$$\phi_4 = \sum_{n=0}^{\infty} \{\bar{\xi}_4^{2n} \cos(2n\theta_O) J_{2n}(kr) + \varepsilon_4^{2n+1} \sin((2n + 1)\theta_O) J_{2n+1}(kr)\} \tag{34}$$

Within the channel of width $2b$ and length ℓ, the velocity potential is

$$\Phi_2(x, y, z, t) = \text{Re}\left\{\phi_2(x, y) \frac{\cosh k(h + z)}{\cosh(kh)} e^{-i\omega t}\right\}$$

where

$$\phi_2 = \sum_{n=0}^{\infty} (\xi_{2,n} e^{i\beta(\lambda_n)x} + \bar{\xi}_{2,n} e^{-i\beta(\lambda_n)(x-\ell)}) \cos \lambda_n y \tag{35}$$

for $0 \leq x \leq \ell$, $-b \leq y \leq b$

$$\beta(\lambda_n) = \sqrt{k^2 - (\lambda_n)^2}$$

where

$$-\lambda_n \tan(\lambda_n b) = i\gamma$$

and γ = damping factor describing the effects of the sidewall. This expression comes from the impedance boundary condition as before [(7)]. The complex constant γ, which is the wave number times the specific admittance of the sidewalls, in one field experiment was found to be on the order of 0.005 to 0.05 (real), from Dalrymple (1992).

The first terms of ϕ_2, with amplitudes $\xi_{2,m}$, represent waves propagating down the straight channel (in the $+x$-direction); the second set of terms (proportional to $\xi_{2,m}$) are waves that are reflected back from the end of the channel.

In the buffer domain of the bay ($x > l$, $0 < r_1 < b$, $0 < \theta_B < \pi$), where $r_1 = \sqrt{(x - \ell)^2 + y^2}$, the wave field has the same form as in the ocean buffer domain

$$\phi_5 = \sum_{n=0}^{\infty} \{\bar{\xi}_5^{2n} \cos(2n\theta_B) J_{2n}(kr_1) + \bar{\xi}_5^{2n+1} \sin((2n + 1)\theta_B) J_{2n+1}(kr_1)\} \tag{36}$$

In the bay ($x > \ell$, $r_1 > b$, $0 < \theta_B < \pi$), the wave field is again represented by a Hankel expansion

$$\Phi_3(x, y, z, t) = \text{Re}\left\{\phi_3(x, y) \frac{\cosh k(h + z)}{\cosh(kh)} e^{-i\omega t}\right\}$$

where

$$\phi_3 = \sum_{n=0}^{\infty} \xi_3^{2n} \cos(2n\theta_B) H_{2n}^1(kr_1) \tag{37}$$

To determine the eight sets of unknowns, ξ_α and $\bar{\xi}_\beta$ for $\alpha = 1, 2, 3, 4, 5$ and $\beta = 2, 4, 5$, eight matching conditions are used. The first two are to be satisfied at the boundary between the ocean and ocean buffer ($r = b$, $0 < \theta_O < \pi$); the second pair is satisfied at the mouth of the channel ($x = 0$) between the buffer solution and that of the channel; the third pair is applied at the entrance to the bay ($x = \ell$); and the last pair is applied at the boundary between bay buffer domain and the bay.

The first matching condition requires that the velocities in the radial direction be the same in the ocean and buffer domain at $r = b$

$$\frac{\partial \phi_1}{\partial r} = \frac{\partial \phi_4}{\partial r} \quad \text{at } r = b,\ 0 < \theta_O < \pi \tag{38}$$

The second requirement is that the pressure be continuous between the buffer and the ocean, which can be expressed as

$$\phi_1 = \phi_4 \quad \text{at } r = b,\ 0 < \theta_O < \pi \tag{39}$$

At the mouth of the channel, there are similar relations between ϕ_4 and ϕ_2 (i.e., the velocities in the x-direction are the same and the water surface is continuous across the channel mouth)

$$\frac{\partial \phi_4}{\partial x} = \frac{\partial \phi_2}{\partial x} \quad \text{at } x = 0, \quad |y| < b \tag{40}$$

$$\phi_4 = \phi_2 \quad \text{at } x = 0, \quad |y| < b \tag{41}$$

At the other end of channel, there are similar relations

$$\frac{\partial \phi_2}{\partial x} = \frac{\partial \phi_5}{\partial x} \quad \text{at } x = \ell, \quad |y| < b \tag{42}$$

$$\phi_2 = \phi_5 \quad \text{at } x = \ell, \quad |y| < b \tag{43}$$

$$\frac{\partial \phi_5}{\partial r} = \frac{\partial \phi_3}{\partial r} \quad \text{at } r = b, \quad 0 < \theta_B < \pi \tag{44}$$

$$\phi_5 = \phi_3 \quad \text{at } r = b, \quad 0 < \theta_B < \pi \tag{45}$$

The following reductions are used to perform the matching condition:

$$\frac{\partial}{\partial x} = \frac{\partial}{r\partial\theta} \quad \text{for } \theta_i = 0, \quad i = O, B$$

$$\frac{\partial}{\partial x} = -\frac{\partial}{r\partial\theta} \quad \text{for } \theta_i = \pi, \quad i = O, B$$

Grouping all of the matching conditions together results in eight equations for the eight sets of unknowns. Using the orthogonality of the trigonometric functions, a set of linear equations for all of the unknowns can be determined.

Results of Momoi's Method

Fig. 10 shows an example of the instantaneous wave field of a wave train normally incident on a channel with the following characteristics: the dimensionless width of the channel is $kb = 7.32$; the length of the channel $k\ell = 73.2$; and damping factor is taken as real, $\gamma = 1\ \text{m}^{-1}$. Numerous interesting reflective and diffractive effects are shown in this narrow slice of the ocean/bay system. On the ocean side of the channel, the reflective shoreline leads to a standing wave offshore, except for the area in front of the channel, where the waves are propagating, due to the absence of strong reflection. Within the channel, the curvature of the wave crests is clear with the waves turning into the channel sideways by diffraction caused by the damping at the sidewalls [as identified by Melo and Guza (1991a)]. Finally, the wave train, after undergoing reflections within the channel, exits the channel, and the curved wave crests due to diffraction are clear within the bay.

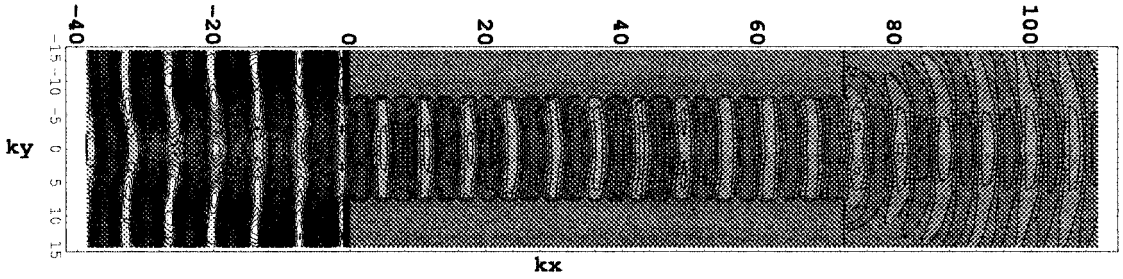

FIG. 10. Plane View of Instantaneous Water Surface Elevation in Rectangular Channel; Ocean at Left, Bay at Right

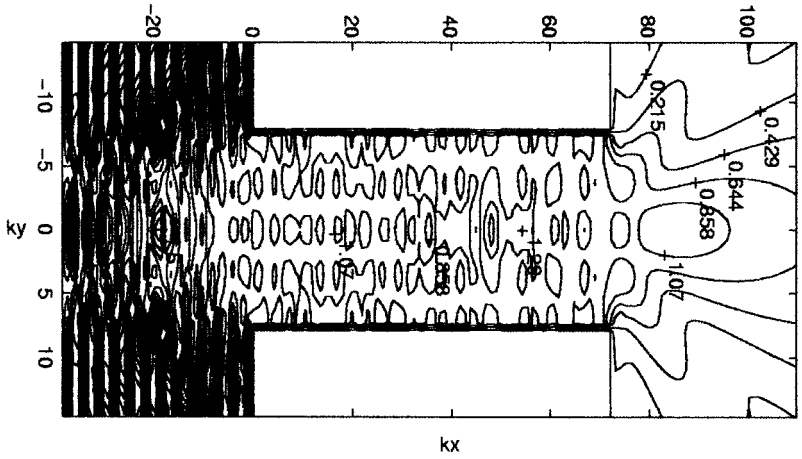

FIG. 11. Absolute Value of Water Surface Elevation; Contours Intervals Are 0.21

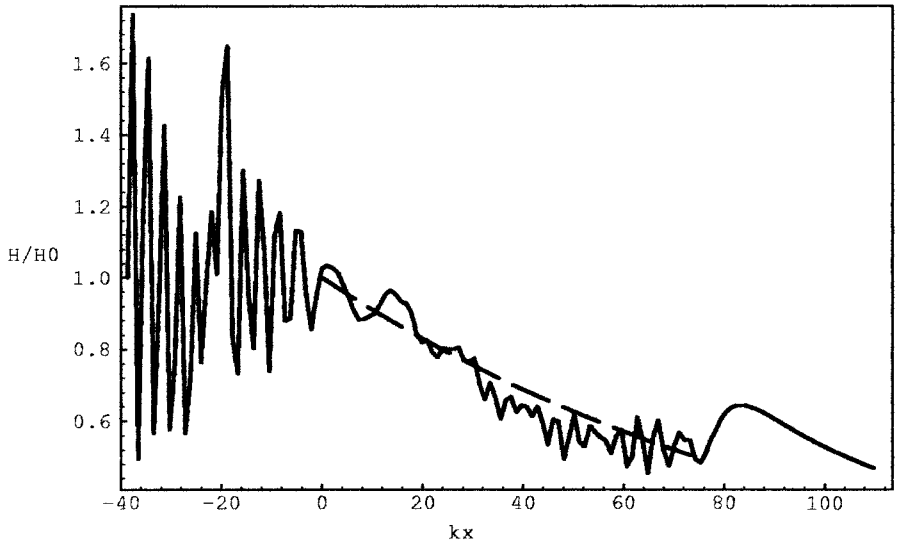

FIG. 12. Decay of Wave Height along Channel Centerline [Sold Line Is Numerical Results; Dashed Line Corresponds to Exponential Decay Predicted by Dalrymple (1992)]; $\gamma = 1\ \text{m}^{-1}$, $kb = 7.32$, $k\ell = 73.2$

The absolute value of the water surface is contoured in Fig. 11, with the contours spaced by 0.12. The initial condition of normally incident waves with unit amplitude leads to a forced phasing of all of the modes that comprise the wave field [(33)], such that there is an amplification of the waves at the ocean side in front of the channel mouth. This amplification differs from the unrealistic amplification exhibited in Dalrymple (1992), where he used a wavemaker condition at the mouth of the channel, leading to a wave focusing just inside the channel.

There is also an amplification of wave energy within the bay due to the diffraction from each corner of the inlet. The diffraction pattern for one side of the inlet is the mirror image of the pattern for the other, and they reinforce down the centerline (The largest contour line shown in the bay corresponds to 1.47, and the smallest is 0.21.)

Fig. 12 shows the decay of the absolute value of the water surface down the central line for this example, and the exponential decay $H = H_0 e^{-\gamma x}$ given by Dalrymple (1992) is also shown (dashed line is the analytical solution, and solid line is the numerical solution). The two solutions compare very well. Fig. 12 also shows the amplification along the centerline within the bay due to the diffractive effects of the inlet ends.

CONCLUSIONS

Two different mathematical treatments in the ocean and bay were used to solve for the wave field in and around an idealized inlet, including reflective and absorbing inlet sidewalls. The first method, used with oblique incidence and reflective sidewalls, leads to a matrix equation that is readily solved for the amplitudes of all wave modes. The extension of this method to more general boundary conditions at the inlet sidewalls leads to intractable Fourier integrals. Therefore, Momoi's buffer domain method, which introduces two additional semicircular domains, permits the ocean and bay wave fields to be expressed in terms of eigenfunction expansions in polar coordinates. More realistic decay down the inlet is shown.

Computed results show that the wave patterns in the channel can vary significantly with angle of incidence and so can the direction of the radiated wave field in the bay. Total energy flux into the bay, however, is almost the same as the amount of energy that illuminates the mouth of the inlet.

APPENDIX I

Dalrymple and Martin (1996) showed that plane wave approximation is good for most values of kb. For a normal incident wave, there is a slight difference between full solution and plane wave approximation for $1 < kb < 2.5$. For the plane wave approximation, the oblique waves in the channel will be neglected; ϕ_2 is now expressed as the leading symmetric wave solution

$$\phi_2(x, y) = \xi^s_{2,0} e^{ikx} + \bar{\xi}^s_{2,0} e^{-ik(x-\ell)} \tag{46}$$

From (21), one has

$$\xi^s_{2,0}(1 + P) + \bar{\xi}^s_{2,0} e^{ik\ell}(1 - P) = \frac{1}{b}\mathcal{L}^s_0(k \sin\theta) = \frac{2 \sin(kb \sin\theta)}{kb \sin\theta} \tag{47}$$

where

$$P = \frac{1}{2} kD^s_{00}/b$$

The equation obtained at the bay mouth [(22)] yields

$$\xi^s_{2,0} e^{ik\ell}(1 - P) + \bar{\xi}^s_{2,0}(1 + P) = 0 \tag{48}$$

Solving these two equations yields

$$\xi^s_{2,0} = \frac{(1 + P)\mathcal{L}^s_0(k \sin\theta)/b}{(1 + P)^2 - (1 - P)^2 e^{2ik\ell}} \tag{49a}$$

$$\bar{\xi}^s_{2,0} = -\frac{(1 - P)e^{ik\ell}\mathcal{L}^s_0(k \sin\theta)/b}{(1 + P)^2 - (1 - P)^2 e^{2ik\ell}} \tag{49b}$$

The long-wave approximation can be found as follows. In D^s_{00}, replace the Hankel function by its small-argument approximation. In this case, $P = kb(1 + 2i(\gamma + \log kb - 3/2)/\pi)$.

The angular dependency of $\xi^s_{2,0}$ and $\bar{\xi}^s_{2,0}$ is very weak, as, for small kb, the $\sin\theta$ terms cancel in $\mathcal{L}^s_0(k \sin\theta)$ [see (47)].

ACKNOWLEDGMENTS

The first and third writers acknowledge the support of the Sea Grant Program of the U.S. Department of Commerce and the Delaware Sea Grant.

APPENDIX II. REFERENCES

Dalrymple, R. A. (1992). "Water wave propagation in jettied channels." *Proc., 23rd Int. Conf. on Coast. Engrg.*, 3040–3053.
Dalrymple, R. A., and Martin, P. A. (1996). "Water waves incident on an infinitely long rectangular inlet." *Appl. Oc. Res.*, 18, 1–11.
Melo, E., and Guza, R. T. (1991a). "Wave propagation in jettied entrance channels. I: Models." *J. Wtrwy., Port, Coast., and Oc. Engrg.*, ASCE, 117(5), 471–492.
Melo, E., and Guza, R. T. (1991b). "Wave propagation in jettied entrance channels. II: Observations." *J. Wtrwy., Port, Coast., and Oc. Engrg.*, ASCE, 117(5), 493–510.
Mendez, O. M., Cadilhac, M., and Petit, R. (1983). "Diffraction of a two-dimensional electromagnetic beam wave by a thick slit pierced in a perfectly conducting screen." *J. Opt. Soc. Am.*, 73, 328–331.
Momoi, T. (1965a). "A long wave in the vicinity of an estuary [I]—An analysis by the method of the buffer domain." *Bull. Earthquake Inst.*, 43, 291–316.
Momoi, T. (1965b). "A long wave in the vicinity of an estuary [II]—An analysis by the method of the buffer domain." *Bull. Earthquake Inst.*, 43, 459–498.
Momoi, T. (1966). "A long wave in the vicinity of an estuary [III]—An analysis by the method of the buffer domain." *Bull. Earthquake Inst.*, 44, 1009–1040.
Momoi, T. (1968). "A long wave in the vicinity of an estuary [IV]." *Bull. Earthquake Inst.*, 46, 631–650.
Park, T. J., Kang, S. H., and Eom, H. J. (1994). "TE scattering from a slit in a thick conducting screen: Revisited." *IEEE Trans. Antennas Propagation*, AP-42, 112–114.
Sneddon, I. N. (1995). *Fourier transforms.*
Stoker, J. J. (1957). *The mathematical theory with applications.*